Journal of Mathematical Chemistry 25 (1999) 111–132

Reaction fronts in an ionic autocatalytic system with an applied electric field

J.H. Merkin [a] and H. Ševčíková [b]

[a] *Department of Applied Mathematics, University of Leeds, Leeds LS2 9JT, UK*
E-mail: amtjhm@amsta.leeds.ac.uk
[b] *Center for Nonlinear Dynamics of Chemical and Biological Systems, Prague Institute of Chemical Technology, Technicka 5, 166 28 Prague 6, Czech Republic*
E-mail: hanka@tiger.vscht.cz
Received 27 July 1998; revised 4 December 1998

The effects of applying an electric field to an ionic autocatalytic reaction with a cubic rate law are discussed. The constant field strength approximation is made and the resulting equations for the model examined by first considering the corresponding travelling wave equations. These show ranges of field strength over which travelling waves do not exist, these ranges being dependent on whether $D > 1$ or $D < 1$, where D is the ratio of diffusion coefficients of autocatalyst and substrate. Numerical simulations of the full system are obtained and these show that, when travelling waves exist, these are formed as the long time behaviour of the system. When travelling waves do not exist, complete electrophoretic separation of the reacting ionic species results, forming separate fronts in autocatalyst and substrate, their direction of propagation depending on D. Comparisons with a related problem with a quadratic rate law are made and the implications for experiments based on the iodate–arsenous acid reaction assessed.

1. Introduction

In a series of recent papers [12,19,21–23] we have considered the effects that applying an electric field can have on the reaction fronts that propagate in a simple autocatalytic system. The basis for these models was a reaction, with a quadratic rate law, between two ionic components, a substrate A^+ and an autocatalyst B^+ (say). Further non-reacting species were also included in the model, with at least one more negatively charged species being necessary to maintain electroneutrality. The system was subjected to an applied electric field through the current being maintained at a constant value.

In [22,23] we considered the basic three-species model where we showed that, depending on the strength and direction of the applied electric field and whether $D > 1$ or $D < 1$ (where $D = D_B/D_A$ is the ratio of the diffusion coefficients of autocatalyst (D_B) and substrate (D_A)), considerable modifications were possible to the front wave which would propagate in the absence of the electric field. These effects included propagating electrophoresis waves where the reaction is virtually ex-

tinguished, wave splitting whereby two, counter-propagating reaction fronts develop, and, in relatively strong fields with $D < 1$, a new type of travelling front propagating against the direction induced by the applied field and in which large concentrations of both substrate and autocatalyst (and hence a much enhanced reaction rate) are achieved.

The effects of including further ionic components were considered in [19,21] where it was shown that there is a transition from the behaviour observed in the three-species model to that which results when the high ionic strength approximation is made. In this approximation the reacting species are assumed to make only a small contribution to the overall ionic balance, allowing the electric field to be taken as a constant. This approximation is used extensively in modelling electric field effects on kinetically more complex systems. A formal justification for making this approximation has been given in [12], where the implications for the autocatalytic model were fully discussed. An additional feature present in these slightly more extended models is the possibility of complete electrophoretic separation of the reacting components. A variant of our original model, in which the autocatalyst is a non-ionic species, has been treated in [3]. In this case wave separation and stopping are seen, whereby electrophoretic separation of substrate and autocatalyst occurs with a stationary front in the autocatalyst being formed.

All these previous studies were based on quadratic autocatalysis. This gave the advantage of being able to calculate the wave speed explicitly from the travelling wave equations, using essentially a minimum-speed criterion. Thus the conditions for the non-existence of kinetic fronts could readily be found with the behaviour in these cases then determined from numerical simulations of the original initial-value problem. Here we consider the analogous problem with cubic autocatalytic kinetics and, for simplicity, we make the high ionic strength (constant field) approximation. We start by considering the travelling wave equations, which we now have to solve numerically to determine the wave speed as well as the conditions for the existence of solution (again finding qualitatively different forms depending on whether $D > 1$ or $D < 1$). We concentrate mostly on the differences between the present case and the corresponding model with quadratic autocatalytic kinetics [12]. We then complement this discussion with numerical simulations of the initial-value problem, paying particular attention to cases where we have predicted that travelling wave solutions do not exist. Finally, we assess the consequences of our theoretical predictions from our simple model for the experimental observations on electric field effects on propagating fronts in the iodate–arsenous acid reaction.

2. Equations

We consider a cubic autocatalytic reaction between the ionic chemical species A^+ and B^+, namely

$$A^+ + 2B^+ \rightarrow 3B^+, \quad \text{rate } kab^2, \tag{1}$$

in a reactor which is taken to be one-dimensional with the electric field being applied in the positive x-direction. The governing equations are derived from the mass balance equations for general reacting ionic systems given by Snita and Marek [20], coupled with the assumption of local electroneutrality. The ionic strength of the reaction mixture is assumed to be sufficiently large for the constant field approximation to be made. The resulting equations are made dimensionless using a_0, the initial (constant) concentration of the substrate A^+, as a concentration scale, and then using $(ka_0^2)^{-1}$ and $(D_A/ka_0^2)^{1/2}$ as time and length scales, respectively. This leads to the (dimensionless) equations

$$\frac{\partial a}{\partial t} = \frac{\partial^2 a}{\partial x^2} - E\frac{\partial a}{\partial x} - ab^2, \tag{2}$$

$$\frac{\partial b}{\partial t} = D\frac{\partial^2 b}{\partial x^2} - DE\frac{\partial b}{\partial x} + ab^2 \tag{3}$$

in terms of the constant (dimensionless) electric field E (which can be either positive or negative) and where $D = D_B/D_A$. A more detailed derivation of the equations for our model is provided in [12,19,23] (with an obvious change from quadratic to cubic autocatalysis) and with a full justification for making the constant field approximation being given in [12].

The initial conditions that we take in the numerical simulations are that

$$a = 1 \quad \text{at } t = 0, \text{ for all } x, \tag{4}$$

with some B^+ introduced locally. We then allow two symmetric, counter-propagating waves to develop fully before the electric field is switched on. This is how previous experiments on electric field effects on reaction systems were conducted (see [15–17,21], for example). It also allows us to treat both positive and negative values of E in the same numerical simulation, the effect of positive E being seen on the waves propagating to the right (positive x-direction) and the effect of negative E on waves propagating to the left in the negative x-direction. Finally, we assume that the reactor is sufficiently long for end effects to be neglected, applying the boundary conditions

$$\frac{\partial a}{\partial x} \to 0, \quad \frac{\partial b}{\partial x} \to 0, \quad \text{as } |x| \to \infty, \ t > 0. \tag{5}$$

However, before we discuss the numerical simulations we consider the travelling wave equations arising from equations (2), (3). Our previous studies [3,12, 19,21–23] have shown that a consideration of the appropriate travelling wave equations is a necessary prerequisite for understanding and interpreting the results of the numerical simulations. We find that similar considerations apply here.

3. Travelling waves

A travelling wave of permanent form is a nonnegative, nontrivial solution to equations (2), (3) written in terms of the single travelling co-ordinate $\zeta = x - vt$, where v is the constant wave speed, approaching uniform concentrations at its rear. This leads us to consider the ordinary differential equations

$$a'' + (v - E)a' - ab^2 = 0, \tag{6}$$

$$Db'' + (v - DE)b' + ab^2 = 0 \tag{7}$$

on $-\infty < \zeta < \infty$ (where primes denote differentiation with respect to ζ).

We assume that the wave is propagating into the unreacted part of the reactor. The conditions to be satisfied ahead of the wave are then

$$a \to 1, \quad b \to 0 \quad \text{as } \zeta \to \infty. \tag{8}$$

Boundary condition (8) then leads, from equation (7), to the requirement that

$$v - DE > 0. \tag{9}$$

It is readily established, using methods deployed previously for similar travelling wave equations [2,9,12], that

$$a \not\equiv 1, \quad b \not\equiv 0 \quad \text{in the wave}, \tag{10}$$

$$a > 0, \quad b > 0 \quad \text{on } -\infty < \zeta < \infty. \tag{11}$$

We now determine the conditions that must hold at the rear of the wave. We assume that $a \to a_s$, $b \to b_s$ as $\zeta \to -\infty$ (where at least one of the constants a_s, b_s must be zero). If we now apply $\int_{-\infty}^{\infty} \ldots \mathrm{d}\zeta$ to equation (7) and use boundary condition (8) and result (11), we obtain

$$(v - DE)b_s = \int_{-\infty}^{\infty} ab^2 \,\mathrm{d}\zeta > 0. \tag{12}$$

From (9) it then follows that $b_s > 0$ and, consequently, that

$$a \to 0, \quad b \to b_s \quad \text{as } \zeta \to -\infty, \tag{13}$$

where b_s is some constant concentration of B^+ to be determined and which will depend on the parameters of the system.

If we now apply $\int_{-\infty}^{\infty} \ldots \mathrm{d}\zeta$ to equation (6), using boundary conditions (8), (13), we obtain

$$(v - E) = \int_{-\infty}^{\infty} ab^2 \,\mathrm{d}\zeta > 0, \tag{14}$$

which provides a stronger condition than (9) if $D < 1$. Conditions (9), (14) and result (11) also allow us, by writing equations (6), (7) in the form

$$\begin{aligned} a' &= \mathrm{e}^{-(v-E)\zeta} \int_{-\infty}^{\zeta} \mathrm{e}^{(v-E)\overline{\zeta}} ab^2 \,\mathrm{d}\overline{\zeta}, \\ b' &= -\frac{1}{D} \exp\left(-\frac{(v-DE)\zeta}{D}\right) \int_{-\infty}^{\zeta} \exp\left(\frac{(v-DE)\overline{\zeta}}{D}\right) ab^2 \,\mathrm{d}\overline{\zeta}, \end{aligned} \tag{15}$$

to establish that

$$a' > 0, \quad b' < 0 \quad \text{on } -\infty < \zeta < \infty. \tag{16}$$

A further result can be obtained if we add equations (6), (7), integrate once with respect to ζ and apply boundary conditions (8), to get

$$a' + Db' + (v-E)a + (v-DE)b = (v-E). \tag{17}$$

Applying boundary conditions (13) then gives

$$b_s = \frac{v-E}{v-DE} = 1 + \frac{(D-1)E}{v-DE}. \tag{18}$$

Expression (18), with (9), shows that $b_s > 1$ if $D > 1,\ E > 0$ or $D < 1,\ E < 0$ and that $b_s < 1$ if $D > 1,\ E < 0$, or $D < 1,\ E > 0$.

To calculate the wave speed v for general values of D and, hence, b_s from expression (18), we have to solve equations (7), (17) numerically. However, before we do so we consider the case $D = 1$, which is reducible to a standard form.

3.1. Special case, $D = 1$

With $D = 1$ we can add equations (6), (7) and obtain the linear equation

$$w'' + (v-E)w' = 0 \tag{19}$$

for $w \equiv a + b$, subject to the boundary conditions (from (8), (18))

$$w \to 1 \quad \text{as } |\zeta| \to \infty. \tag{20}$$

The solution of equation (19) subject to (20) is simply

$$w \equiv 1, \quad \text{i.e.,} \quad a + b \equiv 1. \tag{21}$$

This enables equations (6), (7) to be reduced to the single equation

$$b'' + (v-E)b' + (1-b)b^2 = 0 \tag{22}$$

subject to the boundary conditions

$$b \to 1 \quad \text{as } \zeta \to -\infty, \qquad b \to 0 \quad \text{as } \zeta \to \infty. \tag{23}$$

Equation (22) subject to (23) is the standard cubic Fisher equation (see [1,14], for example) which has the solution

$$v = \frac{1}{\sqrt{2}} + E, \qquad b(\zeta) = \frac{1}{1 + \mathrm{e}^{\zeta/\sqrt{2}}}, \qquad a(\zeta) = \frac{\mathrm{e}^{\zeta/\sqrt{2}}}{1 + \mathrm{e}^{\zeta/\sqrt{2}}}. \tag{24}$$

The form for v given by (24) shows that we must have

$$E > -\frac{1}{\sqrt{2}} \tag{25}$$

for the existence of forward-propagating travelling waves in this case. We also note that (24) gives a linear relation connecting the wave speed v with E.

3.2. General case, $D \neq 1$

To determine v and hence b_s for the general case, $D \neq 1$, we have to solve equations (7), (17) numerically subject to boundary conditions (8), (13), (18). As in previous studies on travelling waves in cubic autocatalytic systems [1], we need to consider the behaviour of the solution close to the front of the wave (where the stationary state (1,0,0) in (a, b, b') travelling wave phase-space has a zero eigenvalue). We require the solution to enter this stationary state on the stable manifold associated with the strictly negative eigenvalue, i.e., in effect requiring that the stationary state be approached through terms which decay exponentially as $\zeta \to \infty$. This restriction is built into our numerical computations (and is implicit in solution (24) for $D = 1$). This results in a single wave speed v being calculated from the solution of the non-linear eigenvalue problem (7), (8), (13), (17) for a given set of parameter values. This is in contrast to the quadratic autocatalysis case [3,12,19,21–23] where the corresponding problem for the travelling waves is satisfied by a continuous spectrum of wave speeds. The initial-value problem then determines which of these speeds is attained in a particular case, usually selected via some "minimum-speed" criterion.

Our previous work on travelling waves in ionic autocatalytic systems [3,12,19,21–23] has shown that qualitatively different behaviour is observed depending on whether $D > 1$ or $D < 1$. The solution for $D = 1$ given above also suggests that this could be a "switch-over" value. This leads us to consider representative values for D for each case.

For the case $D > 1$ we took a value of $D = 2.0$. The results are shown in figure 1(a) (plots of v against E). There are several points to note about the results shown in this figure. There is a (negative) value of E (E_0 say) at which $v = 0$. There is also a lower bound on E (E_c say, with $E_c < E_0$ and where we expect E_0 and E_c to depend on D) for the existence of solutions, i.e., the travelling wave equations have a solution only for $E \geqslant E_c$. For $D = 2.0$ we find that $E_c = -0.355$ (with $v_c = -0.06$). For $E_c < E < 0$ there are two solution branches, with the lower solution branch terminating with $v \to 0$ as $E \to 0^-$. There is no upper bound on E for the existence of solution with, for $E > 0$, v increasing monotonically as E increases. Hence we can

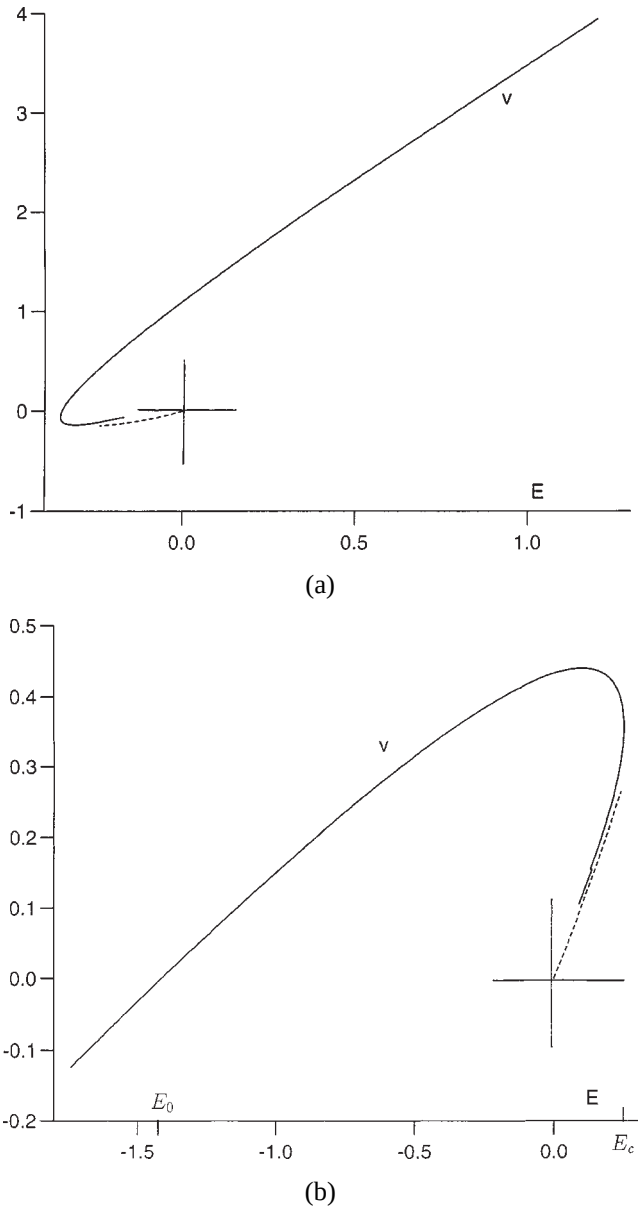

Figure 1. Plots of v against E, obtained from the numerical integration of the eigenvalue problem (7), (8), (13), (17) for the travelling waves for (a) $D = 2.0$, (b) $D = 0.5$. Asymptotic expressions (52) and (51) are shown by the broken lines. E_0 is the value of E at which $v = 0$ (given by (29)), E_c is the bound on E for the existence of travelling wave solutions.

get forward-propagating travelling waves only for $E > E_0$. The single (lower) bound on E for the existence of solutions is similar to the quadratic autocatalysis case [12], though in this latter case there is a simple linear relation connecting v with E.

For the case $D < 1$ we took a value $D = 0.5$. The results are shown in figure 1(b). The main point to note about the results shown in this figure is that now there is only a finite range of E for the existence of forward-propagating travelling waves, with these being possible only for E in the range $E_0 \leqslant E \leqslant E_c$. $E_0 < 0$ (as before), but now $E_c > 0$, for $D = 0.5$ we find that $E_c = 0.251$ (with $v_c = 0.36$). In this respect the behaviour is similar to the quadratic autocatalysis case [12]. For $0 < E < E_c$ there are two solution branches, with the lower branch terminating with $v \to 0$ as $E \to 0^+$. The solution continues smoothly through E_0 with $v < 0$ for $E < E_0$ and $|v|$ increasing monotonically as $|E|$ increases. We shall see from numerical integrations of the initial-value problem described below that the upper branch solutions for v are stable while those on the lower branch are unstable.

We can calculate E_0 directly. To do so we put

$$b = \frac{\overline{b}}{D}, \qquad \overline{\zeta} = \frac{\zeta}{D}, \qquad E_0 = \frac{\overline{E}_0}{D}$$

in equations (6), (7) with $v = 0$ and leave a unscaled. This leads to the equations

$$a'' + \left|\overline{E}_0\right| a' - a\overline{b}^2 = 0, \tag{26}$$

$$\overline{b}'' + \left|\overline{E}_0\right| \overline{b}' + a\overline{b}^2 = 0 \tag{27}$$

(where primes now denote differentiation with respect to $\overline{\zeta}$) subject to the boundary conditions (from (18))

$$a \to 1, \quad \overline{b} \to 0 \quad \text{as } \overline{\zeta} \to \infty, \qquad a \to 0, \quad \overline{b} \to 1 \quad \text{as } \overline{\zeta} \to -\infty. \tag{28}$$

Equations (26), (27) subject to (28) are essentially the standard cubic Fisher problem for equal diffusivities [1,14] and have essentially the solution given by (24). Thus we can conclude that

$$E_0 = -\frac{1}{\sqrt{2}D}. \tag{29}$$

Note that result (29) agrees with (25) when $D = 1$. The corresponding result for the quadratic autocatalysis case [12] is $E_0 = -2/\sqrt{D}$, having a different functional dependence on the diffusion coefficient ratio D.

Asymptotics

The numerical solutions of the travelling wave problem have identified several asymptotic regimes, namely the form of the wave speed for large (positive or negative) fields and the behaviour of the lower branch solutions as $|E| \to 0$. We start by considering the case of strong fields, discussing the cases $D > 1$ and $D < 1$ separately.

(i) $D > 1$, E large ($E > 0$). We can obtain a solution of equations (6), (7) for $D > 1$ valid for E large by first writing

$$v = DE + E^{1/3}V, \qquad b = E^{2/3}B, \qquad Y = E^{1/3}\zeta \tag{30}$$

and leaving a unscaled. This leads to the equations

$$(D-1)a' - aB^2 + E^{-2/3}\big(a'' + Va'\big) = 0, \tag{31}$$

$$DB'' + VB' + aB^2 = 0 \tag{32}$$

(where primes now denote differentiation with respect to Y) subject to

$$\begin{aligned} &a \to 1, \quad B \to 0 \quad \text{as } Y \to \infty, \\ &a \to 0, \quad B \to \frac{(D-1) + E^{-2/3}V}{V} \quad \text{as } Y \to -\infty. \end{aligned} \tag{33}$$

An expansion in powers of $E^{-2/3}$ is suggested. The leading order problem becomes, after the further transformation,

$$B = \left(\frac{D-1}{V}\right)\widetilde{B}, \qquad \widetilde{Y} = \left(\frac{D-1}{DV}\right)^{1/2} Y,$$

$$\begin{aligned} V_1 a' - a\widetilde{B}^2 &= 0, \\ \widetilde{B}'' + V_1\widetilde{B}' + a\widetilde{B}^2 &= 0, \end{aligned} \tag{34}$$

subject to

$$\begin{aligned} &a \to 1, \quad \widetilde{B} \to 0 \quad \text{as } \widetilde{Y} \to \infty, \\ &a \to 0, \quad \widetilde{B} \to 1 \quad \text{as } \widetilde{Y} \to -\infty, \end{aligned} \tag{35}$$

and where

$$V_1 = \frac{V^{3/2}}{(D(D-1))^{1/2}}.$$

The system given by equations (34), (35) is the same as that has arisen previously [13] from which we obtain a value for V_1 as $V_1 = 0.8609$. This gives

$$v \sim DE + 0.9050\big(D(D-1)E\big)^{1/3} + \cdots \quad \text{as } E \to \infty \text{ for } D > 1. \tag{36}$$

From expressions (18), (36) we then obtain

$$b_s \sim 1.105\frac{(D-1)^{2/3}}{D^{1/3}}E^{2/3} + \cdots \quad \text{as } E \to \infty. \tag{37}$$

For $D = 2.0$, expressions (36), (37) become

$$v \sim 2E + 1.1402E^{1/3} + \cdots, \quad b_s \sim 0.877E^{2/3} + \cdots \quad \text{as } E \to \infty.$$

(ii) $D < 1$, $|E|$ large ($E < 0$). A similar argument, with essentially the same scalings (replacing E with $|E|$), can be applied to the case when $D < 1$ for large, negative E. Here we find that

$$v \sim DE + 0.9050\big(D(1-D)\big)^{1/3}|E|^{1/3} + \cdots \quad \text{as } E \to -\infty \tag{38}$$

with v being negative for E large and negative. Applying (38) in (18) gives

$$b_s \sim 1.105\frac{(1-D)^{2/3}}{D^{1/3}}|E|^{2/3} + \cdots \quad \text{as } |E| \to \infty. \tag{39}$$

For $D = 0.5$, expressions (38), (39) give

$$v \sim 0.5E + 0.5701|E|^{1/3} + \cdots, \quad b_s \sim 0.877|E|^{2/3} + \cdots \quad \text{as } E \to -\infty.$$

We now consider how the lower branch solutions terminate as $|E| \to 0$, again treating the cases $D < 1$ and $D > 1$ separately.

(iii) $E \to 0^+$, $D < 1$, on the lower solution branch. To determine the behaviour of the solution on the lower branch as $E \to 0^+$ for $D < 1$, we start in an inner region where we put

$$v = E + E^2\widehat{V}, \qquad a = E\widehat{A}, \qquad b = E\widehat{B}, \qquad \widehat{Y} = E\zeta.$$

This leads to the equations

$$\widehat{A}'' - \widehat{A}\widehat{B}^2 + E\widehat{V}\widehat{A}' = 0, \tag{40}$$

$$D\widehat{B}'' + (1-D)\widehat{B}' + \widehat{A}\widehat{B}^2 + E\widehat{V}\widehat{B}' = 0, \tag{41}$$

subject to the boundary conditions

$$\widehat{A} \to 0, \quad \widehat{B} \to \frac{\widehat{V}}{(1-D) + E\widehat{V}} \quad \text{as } \widehat{Y} \to -\infty, \qquad \widehat{B} \to 0 \quad \text{as } \widehat{Y} \to \infty. \tag{42}$$

The condition on $\widehat{A}$ as $\widehat{Y} \to \infty$ will be satisfied later.

An expansion in powers of E is suggested, the leading order problem $(\widehat{A}_0, \widehat{B}_0, \widehat{V}_0)$ satisfying, after the further transformation,

$$\widehat{A}_0 = (1-D)\overline{A}_0, \qquad \widehat{B}_0 = \frac{(1-D)}{D}\overline{B}_0, \qquad \overline{Y} = \frac{(1-D)}{D}\widehat{Y},$$

the equations

$$\overline{A}_0'' - \overline{A}_0\overline{B}_0^2 = 0, \tag{43}$$

$$\overline{B}_0'' + \overline{B}_0' + \overline{A}_0\overline{B}_0^2 = 0, \tag{44}$$

subject to the boundary conditions

$$\overline{A}_0 \to 0, \quad \overline{B}_0 \to \frac{D\widehat{V}_0}{(1-D)^2} \quad \text{as } \overline{Y} \to -\infty, \qquad \overline{B}_0 \to 0 \quad \text{as } \overline{Y} \to \infty. \tag{45}$$

The numerical solution of equations (43)–(45) gives

$$\frac{D\widehat{V}_0}{(1-D)^2} = 0.82066 = c_0$$

and has

$$\overline{A}_0 \sim c_0\overline{Y} + d_0 \quad \text{as } \overline{Y} \to \infty, \text{ where } d_0 = 0.98338.$$

The above expression shows that the expansion is non-uniform and to determine the scalings for an outer region we need to consider the terms of O(E). The details are not important, finding that

$$\widehat{A}_1 \sim \frac{-\widehat{V}_0^2\widehat{Y}^2}{2} + \left(\widehat{V}_1 - d_0\widehat{V}_0\right)\widehat{Y} + d_1, \quad \widehat{B}_1 \to 0 \quad \text{as } \widehat{Y} \to \infty. \tag{46}$$

Equation (46) shows that the non-uniformity occurs where $\widehat{Y}$ is O(E^{-1}) (i.e., where ζ is O(E^{-2}). In the outer region we then put

$$\xi = E^2\zeta, \qquad b \equiv 0 \tag{47}$$

and leave a unscaled. This leads to the problem at leading order in the outer region

$$a'' + \widehat{V}_0 a' = 0, \tag{48}$$

subject to, on matching with the solution in the inner region,

$$a \sim \widehat{V}_0\xi - \frac{\widehat{V}_0^2\xi^2}{2} + \cdots \quad \text{as } \xi \to 0, \qquad a \to 1 \quad \text{as } \xi \to \infty. \tag{49}$$

The required solution is

$$a = \left(1 - \mathrm{e}^{-\widehat{V}_0\xi}\right). \tag{50}$$

From the above we then have that

$$\begin{aligned} v &\sim E + 0.82066\frac{(1-D)^2E^2}{D} + \cdots, \\ b_s &\sim 0.82066\frac{(1-D)}{D}E + \cdots \quad \text{as } E \to 0^+ \end{aligned} \tag{51}$$

on the lower solution branch. Asymptotic result (51) is also shown in figure 1(b) (by the broken line).

(iv) $E \to 0^-$, $D > 1$, on the lower solution branch. A similar argument to that given above can be used to describe the solution on the lower branch as $E \to 0^-$ for the case $D > 1$, in effect using $|E|$ for E in the scalings given previously. This leads to the asymptotic expression

$$\begin{aligned} v &\sim E + 0.82066\frac{(D-1)^2E^2}{D} + \cdots, \\ b_s &\sim 0.82066\frac{(D-1)}{D}|E| + \cdots \quad \text{as } E \to 0^-. \end{aligned} \tag{52}$$

Expression (52) is also shown in figure 1(a) (by the broken line).

4. Numerical simulations

The initial-value problem (2)–(5) subject to the initial conditions described above was solved numerically using a standard Crank–Nicolson implicit scheme for parabolic systems. In this forward differences are used to approximate the time derivatives and the other terms averaged over the time step t to $t + \Delta t$. The space derivatives are then replaced by central differences and the two sets of nonlinear algebraic equations that result solved by Newton–Raphson iteration. This procedure was found to converge easily in all the calculations performed. A space step of $\Delta x = 0.1$ was used throughout and an adjustable time step Δt was used to maintain accuracy (Δt is determined by covering each time step with first one and then two integrations and choosing Δt so that the difference in the two solutions was pointwise less than 5×10^{-4}).

Our discussion of the travelling wave equations has revealed that different criteria for the existence of these waves apply for $D > 1$ and $D < 1$. We consider these two cases separately. However, we start with a brief look at the case $D = 1$, where the basic equations (2), (3) can be reduced to standard form.

(i) $D = 1$. Travelling waves were found for all values of E tried, with all these waves having the same shape (i.e., the cubic Fisher solution) though their propagation speeds are different. If condition (25) is satisfied we found that the waves propagated in the same direction as they were before the field was switched on and, if this condition is not satisfied, they reversed direction. This is illustrated in figure 2 (for $E = 1.5$). (In this, and subsequent figures, the concentration profiles shown by the broken lines are the wave profiles at the point that the electric field was switched on.) This is an example where $E < -1/\sqrt{2}$ for the left-propagating wave and we can see that the direction of propagation of this wave has changed. The right-propagating wave has an increased speed. In both cases the wave profiles remain unchanged. The wave speeds

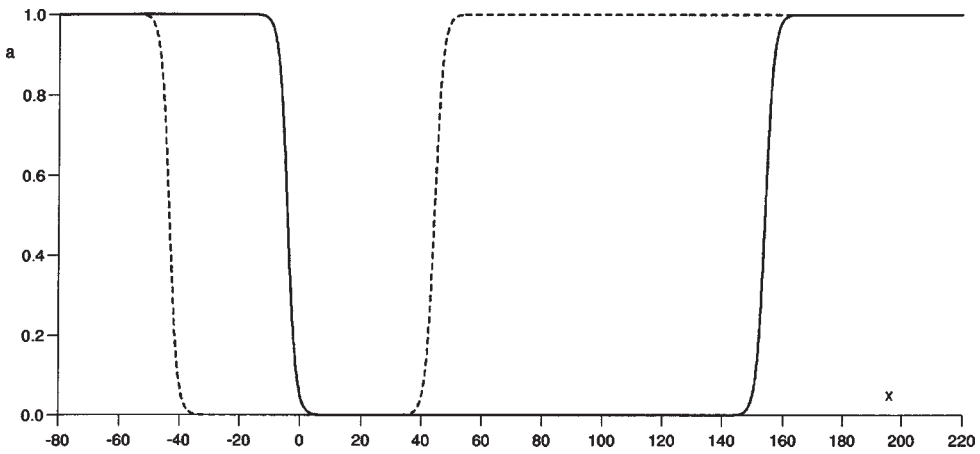

Figure 2. Wave profiles obtained from the numerical solution of the initial-value problem (2)–(5) for $D = 1.0$, $E = 1.5$. The broken lines are the concentration profiles just before the electric field was switched on, at $t = 60.0$. The profiles well after the field has been switched on (full lines) are at $t = 110.3$.

calculated from the numerical solutions all correlated well with the values given by expression (24).

(ii) $D > 1$. Here we took a representative value for D as $D = 2.0$. In this case $E_0 = -0.3536$ with forward-propagating waves being predicted for all $E > E_0$ (figure 1(a)). If we take a value of E such that $-E > E_0$, then travelling waves are formed, propagating in both directions. This is illustrated in figure 3(a), where we plot wave profiles obtained from the numerical simulation for $E = 0.25$. This is a case where the direction of propagation of both waves remains unchanged when the electric field is switched on (here at $t = 50.0$), with the speed of the right-propagating wave increased and that of the left-propagating wave decreased. These speeds were calculated from the numerical simulation as $v_R = 1.722$ (right-propagating wave) and

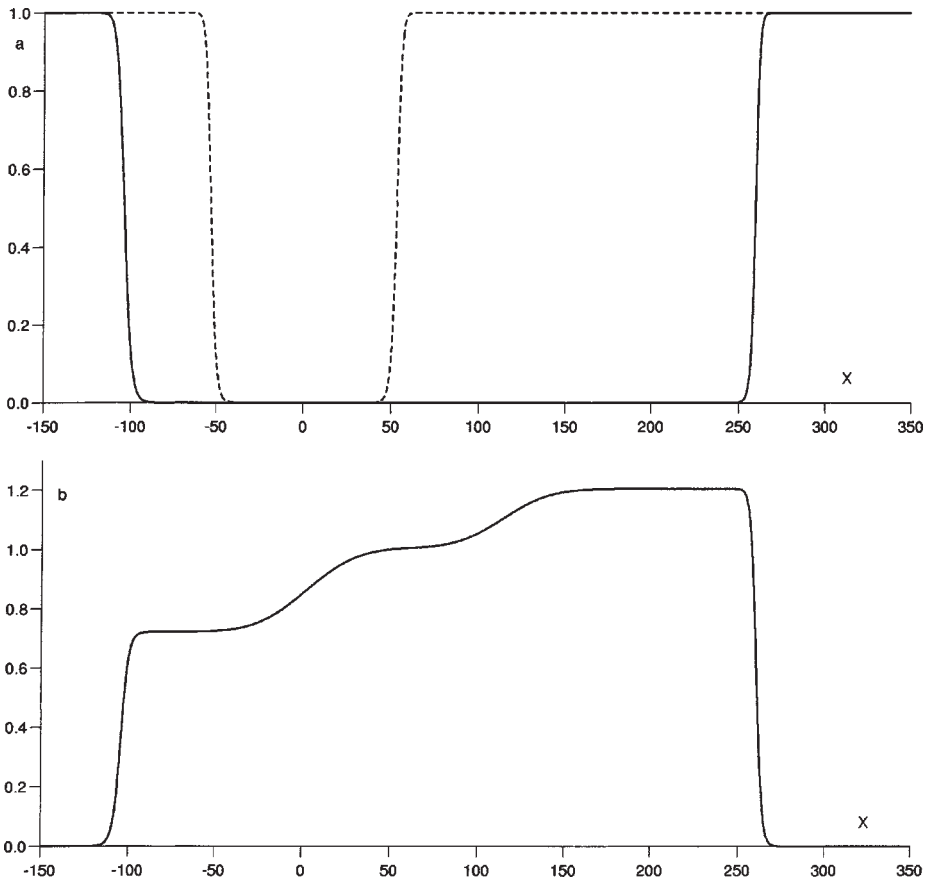

(a)

Figure 3. Wave profiles obtained from the numerical solution of the initial-value problem (2)–(5) for $D = 2.0$. The broken lines are the concentration profiles just before the electric field was switched on, at $t = 50.0$. The profiles well after the field has been switched on (full lines) are for (a) $E = 0.25$ at $t = 170.3$, (b) $E = 0.5$ at $t = 290.1$, (c) $E = 1.5$ at $t = 139.1$.

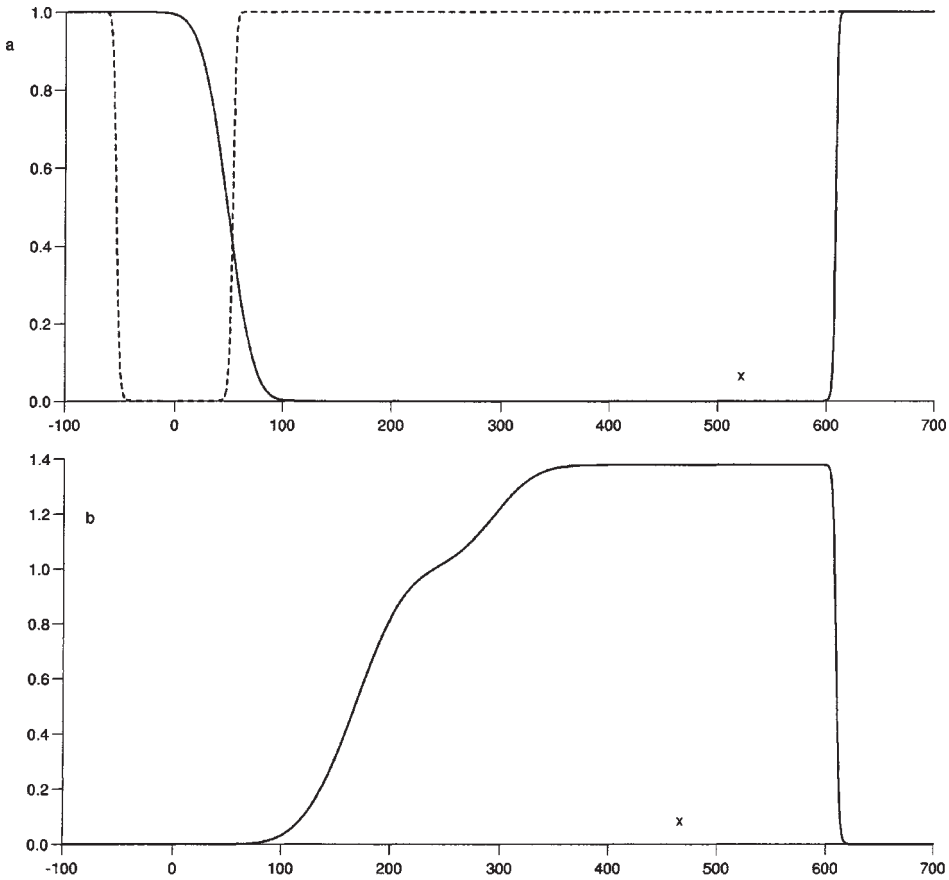

(b)

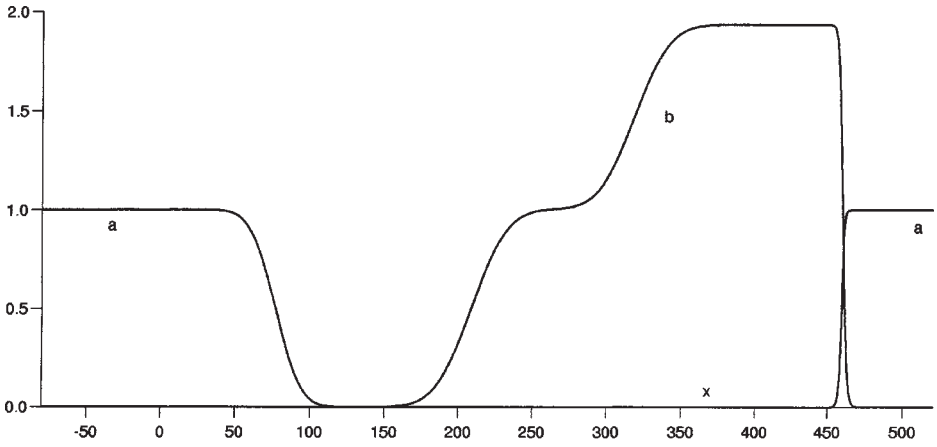

(c)

Figure 3. (Continued.)

$v_{\rm L} = 0.396$ (left-propagating wave) as compared with a wave speed of 1.095 without the electric field. Both $v_{\rm R}$ and $v_{\rm L}$ agree well with the values determined from the travelling wave equations (7), (8), (13), (17). We see that the concentration of B^+ behind the right-propagating wave is increased when the field is switched on, to a value $b_{s,{\rm R}} = 1.205$ and is decreased to $b_{s,{\rm L}} = 0.721$ behind the left-propagating wave. This is in accord with expression (18).

As well as the travelling waves there is also a purely electrophoresis front in B^+ propagating to the right with a speed DE (and spreading slowly by diffusion). In this electrophoretic front the concentration of A^+ is zero (and hence no reaction takes place). The structure of this front is, for t large, given by

$$b \sim 1 + \frac{(b_{s,{\rm R}} - 1)}{\sqrt{\pi}} \int_{-\infty}^{\eta} \exp\bigl(-s^2\bigr)\,{\rm d}s, \quad \eta = \frac{(x - DEt)}{2\sqrt{Dt}}. \tag{53}$$

There is a further, purely diffusive structure in B^+ centred at the origin, in which

$$b \sim b_{s,{\rm L}} + \frac{(1 - b_{s,{\rm L}})}{\sqrt{\pi}} \int_{-\infty}^{\overline{\eta}} \exp\bigl(-s^2\bigr)\,{\rm d}s, \quad \overline{\eta} = \frac{x}{2\sqrt{Dt}}, \tag{54}$$

for t large. It is through these two structures (53), (54) that the differences in the concentrations of B^+ at the rear of the right- and left-propagating waves are accommodated. The wave profiles for the substrate A^+ appear virtually unchanged after the field is switched on.

If we now take a value of E such that $-E < E_c$, we still obtain a travelling wave propagating to the right. This is illustrated in figure 3(b) and (c) for $E = 0.5$ and $E = 1.5$, respectively. The speeds of these waves, as calculated from the numerical simulations, $v_{\rm R} = 2.322$ and $v_{\rm R} = 4.602$, agree well with the speeds determined from the travelling wave equations, as do the concentrations of B^+ at the rear of these waves, $b_{s,{\rm R}} = 1.379$ and $b_{s,{\rm R}} = 1.936$, respectively. Note that $b_{s,{\rm R}}$ increases with E, as suggested by (18) and (37). As before, the wave profiles in A^+ remain virtually unaffected by the electric field.

There is a qualitative change in the structure of the left-propagating wave after the field is switched on. Now electrophoretic separation of substrate A^+ and autocatalyst B^+ occurs, with distinct profiles in these species being formed. The direction of propagation is reversed, these electrophoresis fronts in A^+ and B^+ propagate to the right with speeds $|E|$ and $D|E|$, respectively, becoming increasingly separated as t increases. This is a relatively slow process for $E = 0.5$ (figure 3(b)) where separation has not been fully achieved even at $t = 290.1$, whereas it is much more rapid for larger values of E (figure 3(c)). For t large, the structure of these electrophoresis fronts is given by

$$\begin{aligned} a &\sim \frac{1}{\sqrt{\pi}} \int_{\xi}^{\infty} \exp\bigl(-s^2\bigr)\,{\rm d}s, \quad \xi = \frac{(x - |E|t)}{2\sqrt{t}}, \\ b &\sim \frac{1}{\sqrt{\pi}} \int_{-\infty}^{\overline{\xi}} \exp\bigl(-s^2\bigr)\,{\rm d}s, \quad \overline{\xi} = \frac{(x - D|E|t)}{2\sqrt{Dt}}. \end{aligned} \tag{55}$$

There is (as in figure 3(a)) another electrophoresis front in B^+, whose structure is given by (53) for t large, also propagating to the right with speed DE, through which the higher concentration of B^+ at the rear of the right-propagating travelling wave is achieved.

Finally, we considered a value of E in the (narrow) range $E_c < E < E_0$, where a travelling wave solution exists but has a negative velocity (figure 1(a)). In this case we again find travelling waves after the field has been switched on, the wave propagating to the right having its speed increased. The wave propagating to the left is slowly decelerated until its direction is reversed, finally propagating slowly to the right. This suggests that v going through zero at E_0 does not cause any problem with regard to travelling wave formation and, for $E = E_0$, we will obtain a stationary wave front.

(iii) $D < 1$. Here we took $D = 0.5$, with forward-propagating waves being predicted only for E in the finite range $E_0 < E < E_c$ where, for this case, $E_0 = -1.4142$ ($= -\sqrt{2}$) and $E_c = 0.2511$ (figure 1(b)). For E in this range, travelling waves are initiated, with their direction of propagation unaltered after the electric field is switched on. This is illustrated in figure 4(a) for $E = 0.2$. The wave speeds calculated for this case are $v_{\mathrm{R}} = 0.427$ and $v_{\mathrm{L}} = 0.396$, in agreement with figure 1(b). Note that both of these speeds are less than a speed of 0.435 when no field is applied. This effect is dependent on the value of E chosen, small (positive) values of E accelerate the right-propagating wave, the maximum forward speed occurring at $E = 0.106$ (figure 1(b)). In figure 4(a) we see that, in this case, the concentration of B^+ at the rear of the right-propagating wave is decreased (to $b_{s,\mathrm{R}} = 0.694$) and is increased behind the left-propagating wave (to $b_{s,\mathrm{L}} = 1.202$), as follows from (18). As was found for $D > 1$, the wave profile in the substrate A^+ appears to be mostly unaffected by the electric field.

We next consider a value of E such that $E > E_c$ and $E < |E_0|$. This case is illustrated in figure 4(b) for $E = 1.0$. There is still a travelling wave propagating to the left, with speed $v_{\mathrm{L}} = 0.151$ as calculated from the numerical simulation, with the concentration of B^+ at its rear increased to $b_{s,\mathrm{L}} = 1.768$. However, electrophoretic separation occurs in the right-propagating wave and distinct fronts in A^+ and B^+ are formed. These propagate with speeds E and DE, respectively, and so become increasingly separated as t increases. The structure of these electrophoretic fronts is essentially given by (55) for t large.

If we increase E so that it lies outside the range $E_0 < E < E_c$, then we still have complete electrophoretic separation of A^+ and B^+ formed from the right-propagating wave, as can be seen in figure 4(c) for $E = 2.0$. The difference between this and the previous case (figure 4(b)) is that now the travelling wave formed from the left-propagating wave has its direction of propagation reversed. With the electric field switched on, this propagates to the right with speed $v_{\mathrm{L}} = -0.227$ (having an increased concentration of B^+ at its rear, $b_{s,\mathrm{L}} = 2.294$). This behaviour continues as E is increased still further, with complete electrophoretic separation of the right-propagating wave, so that v passing through zero at $E = E_0$ has only the effect of

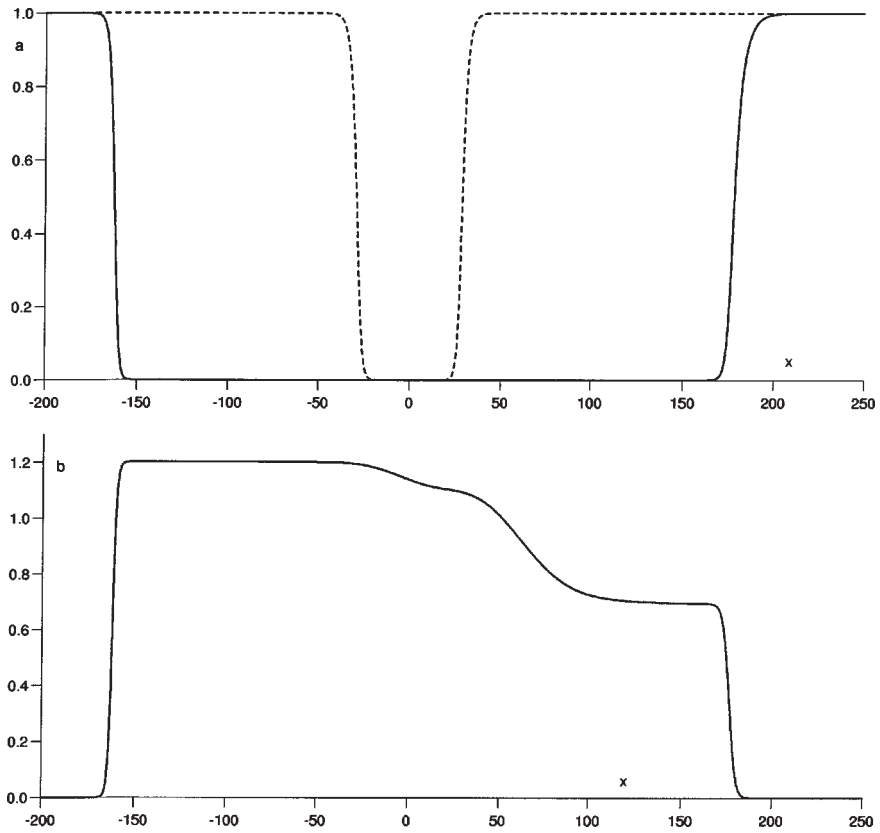

(a)

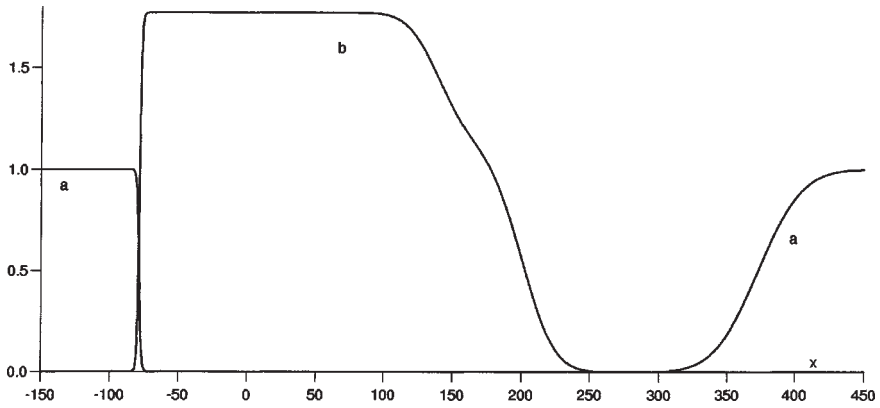

(b)

Figure 4. Wave profiles obtained from the numerical solution of the initial-value problem (2)–(5) for $D = 0.5$. The broken lines are the concentration profiles just before the electric field was switched on, at $t = 60.0$. The profiles well after the field has been switched on (full lines) are for (a) $E = 0.2$ at $t = 400.2$, (b) $E = 1.0$ at $t = 530.8$, (c) $E = 2.0$ at $t = 272.3$.

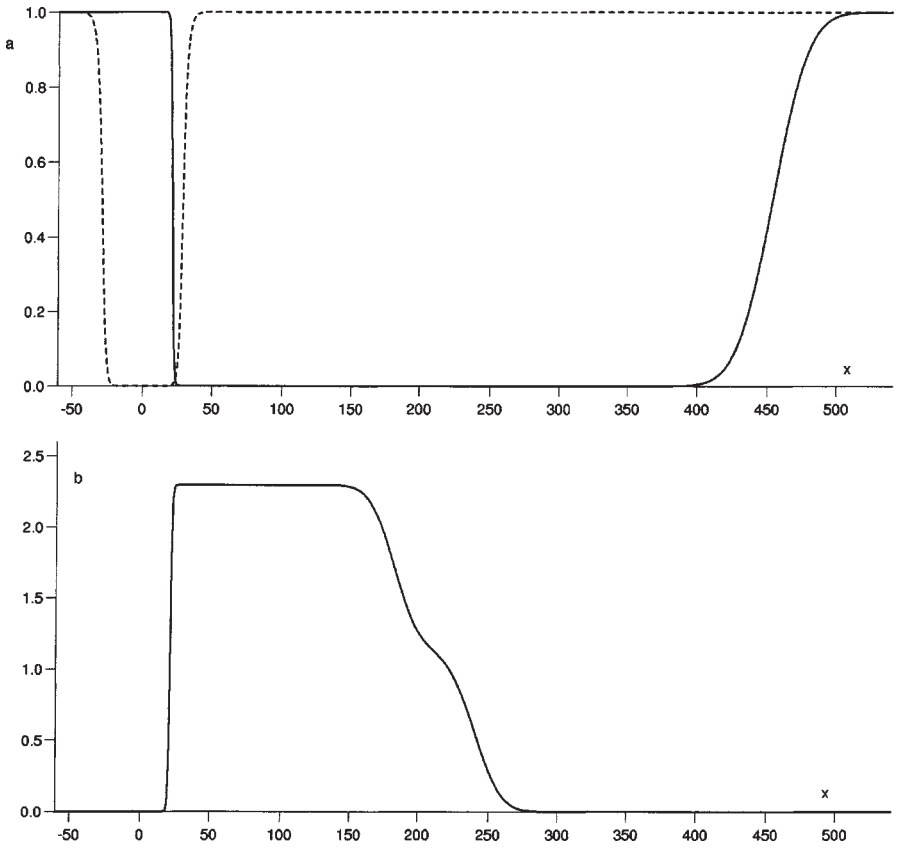

(c)

Figure 4. (Continued.)

reversing the direction of propagation of the initially left-propagating wave and does not produce any further, qualitatively different structures.

To complete this section we compare briefly the results for the present model with those for quadratic autocatalysis [12]. A feature seen here and not in [12] is the range of E over which there are two solutions to the travelling wave equations. All our numerical solutions to initial-value problem (2)–(5) approached the solutions on the upper branch as t increased (for both $D > 1$ and $D < 1$). This suggests that these upper branch solutions are stable and the lower branch solutions temporally unstable. Further numerical integrations, starting with initial conditions close to lower branch wave solutions, moved away from these initial conditions and towards the corresponding upper branch solution, again suggesting that these lower branch solutions are unstable. A similarity with [12] is the complete electrophoretic separation of the A^+ and B^+ profiles. For both quadratic and cubic autocatalysis, these fronts propagate back into the fully reacted region for $D > 1$ and forward into the unreacted region for $D < 1$. A further similarity between the two cases is the existence of travelling waves with

negative velocities. In both cases, this leads to waves whose direction of propagation is reversed, i.e., they propagate back into the already reacted region, after the electric field is switched on.

5. Discussion

The iodate–arsenous acid reaction is one that is used to demonstrate propagating reaction fronts and, when arsenous acid is in stoichiometric excess, the reaction can be effectively modelled by a cubic autocatalytic rate law [6,7,14,18]. The influence of electric fields on fronts propagating in a reactor using this reaction have been reported originally in [15], with the results from a much more extensive study of this system being presented in [4,5]. These latter studies showed particularly clearly that the effects of applying the electric field are strongly dependent on the stoichiometric factor $R = [H_3AsO_3]_0/[IO_3^-]_0$ (the ratio of the initial concentrations of arsenous acid and iodate).

To model the reaction purely by cubic autocatalysis (without an electric field) requires $R > 3$ [10] and it is only this case that we consider here. In figure 5 we show wave speeds V measured from a series of experiments, each with $R = 3.1$, plotted against the applied field $\mathcal{E}$. We note that the ionic species, mainly IO_3^- and I^-, are negatively charged and, hence, the applied field acts in the opposite sense to that in our model. (Alternatively, this is equivalent to a change in sign of E.) The experimental results show that the wave speed is increased with $\mathcal{E}$ negative and decreased with $\mathcal{E}$ positive. This agrees with the results from our model (with the required change in sign of E), see figure 1, for example. There is also a positive field strength at which the wave is brought to rest (in the experiments $V \simeq 0$ at $\mathcal{E} = 5.0$), again in line with our model (expression (29)).

For sufficiently strong positive fields, the final outcome of the reaction taking place within the propagating front can be altered qualitatively [4,5]. This is observed through monitoring the formation of I_2 using starch as an indicator. In the present case, I_2 is an intermediate without the electric field, but in a positive field it can become a reaction product, remaining after the passage of the front. This makes direct comparison with our simple model unreliable, though the trends are the same. This does not happen in negative fields (I_2 is an intermediate in all cases) and so comparisons can be made. Expressions (36), (38) give a linear relation between speed and field strength for strong fields, positive or negative depending whether $D < 1$ or $D > 1$. Figure 5 suggests a linear relation between V and $\mathcal{E}$ for sufficiently large negative values of $\mathcal{E}$ (for $|\mathcal{E}| > 10$). This is consistent with having $D > 1$ (figure 1(a)). The values quoted for the diffusion coefficients of the ionic species [15] give $D \simeq 1.44$, though this value could well be unreliable as it is known that the presence of starch in the reaction mixture can significantly alter the effective diffusion coefficients of these species [8].

A feature seen in our model is the possibility of complete electrophoretic separation of the reacting ionic species. We could expect this feature to be present in the

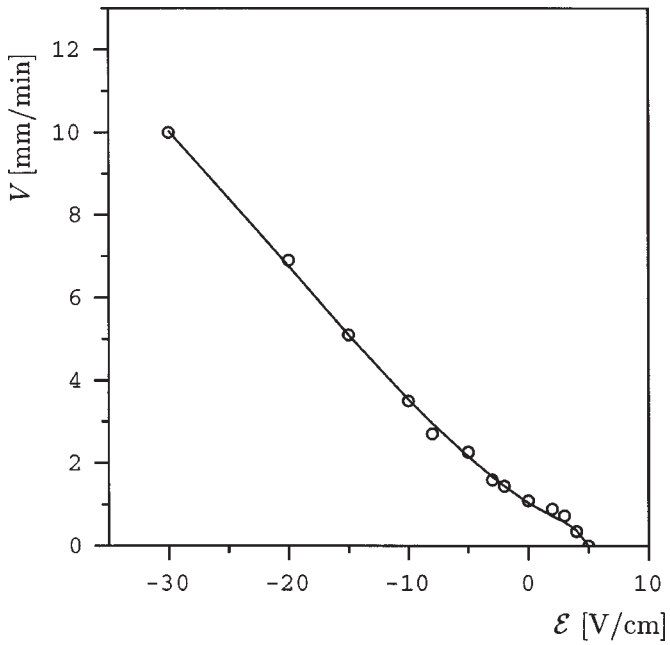

Figure 5. Experimental observations for the iodate–arsenous acid reaction with stoichiometric factor $R = 3.1$, plotting the measured wave speed V (mm/min) against the applied electric field $\mathcal{E}$ (V/cm).

iodate–arsenous acid system and, for this system, it would mean that the reaction had stopped. Thus the production of I_2 (as observed through colour changes in the starch) would cease, giving the appearance that wave propagation had ceased. This feature has been reported in the experiments [15] where it was suggested that the ionic species do become fully separated in relatively high (positive) fields ($\mathcal{E} > 7$ V/cm) (corresponding to negative E in our model). On switching the field off again, the reaction was observed to restart after some further time had elapsed with a wave front being seen initially at approximately the same position as it was when the front ceased to exist. This new front then propagates while the dark zone of non-zero I_2 concentration gets lighter and finally disappears. The electrophoretic separation of the main ionic species seen in our model for sufficiently high field strengths could provide an explanation for this.

The detailed study of the iodate–arsenous acid system [4,5] has revealed that the effects of applying electric fields to propagating waves are much more complex than can be accounted for by a model relying only on a single autocatalytic rate law. This is particularly evident for reaction mixtures which have $R < 3$. A more systematic theoretical treatment, based on more realistic kinetics (the Dushman–Roebuck scheme, for example), is required to unravel all the observed features. This has been undertaken for a prototype two-step system [11] and is, at present, being considered for realistic models of the iodate–arsenous acid kinetics.

Acknowledgements

This work is partly supported by grant VS96073 from MSMT (Ministry of Education, Czech Republic) and a travel grant from the Leverhulme Trust.

References

[1] J. Billingham and D.J. Needham, A note on the properties of a family of travelling-wave solutions arising in cubic autocatalysis, Dynam. Stabil. Syst. 6 (1991) 33–49.
[2] J. Billingham and D.J. Needham, The development of travelling waves in quadratic and cubic autocatalysis with unequal diffusion coefficients. I. Permanent form travelling waves, Philos. Trans. Roy. Soc. London Ser. A 334 (1991) 1–24.
[3] A.B. Finlayson and J.H. Merkin, Travelling waves in an ionic quadratic autocatalytic chemical system, Math. Comput. Modelling, accepted.
[4] L. Forstova, Studium účinků elektrického pole na stechiometrii oxidace kyseliny arsenité jodičnanem v plošném reaktoru [Studies of electric field effects on the stoichiometry of the arsenous acid oxidation by iodate in a planar reactor], M.Sc. dissertation, VSCHT, Prague (1998) (in Czech).
[5] L. Forstova, H. Ševčíková, M. Marek and J.H. Merkin, Electric field effects on the local stoichiometry of front waves, Chem. Eng. Sci., accepted.
[6] A. Hanna, A. Saul and K. Showalter, Detailed studies of propagating fronts in the iodate oxidation of arsenous acid, J. Am. Chem. Soc. 104 (1982) 3838–3844.
[7] D. Horvath and K. Showalter, Instabilities in propagating reaction–diffusion fronts of the iodate–arsenous acid reaction, J. Chem. Phys. 102 (1995) 2471–2478.
[8] I. Lengyel and I.R. Epstein, Modelling of Turing structure in the chlorite–iodide–malonic acid–starch system, Science 251 (1991) 650–652.
[9] J.H. Merkin, D.J. Needham and S.K. Scott, Coupled reaction–diffusion waves in an isothermal autocatalytic chemical system, IMA J. Appl. Math. 50 (1993) 43–76.
[10] J.H. Merkin and H. Ševčíková, Travelling waves in the iodate–arsenous acid system, Phys. Chem. Chem. Phys. 1 (1999) 91–97.
[11] J.H. Merkin, H. Ševčíková and D. Snita, The effect of an electric field on the local stoichiometry of front waves in an ionic chemical system, submitted.
[12] J.H. Merkin, H. Ševčíková, D. Snita and M. Marek, The effects of an electric field on an autocatalytic ionic reaction in a system with high ionic strength, IMA J. Appl. Math. 60 (1998) 1–31.
[13] M.J. Metcalf, J.H. Merkin and S.K. Scott, Oscillating wave fronts in isothermal chemical systems with arbitrary powers of autocatalysis, Proc. Roy. Soc. London Ser. A 447 (1994) 155–174.
[14] A. Saul and K. Showalter, Propagating reaction–diffusion fronts, in: *Oscillations and Travelling Waves in Chemical Systems*, eds. R.J. Field and M. Burger (Wiley–Interscience, New York, 1985).
[15] H. Ševčíková and M. Marek, Chemical front waves in an electric field, Physica D 13 (1984) 379–386.
[16] H. Ševčíková, M. Marek and S.C. Muller, The reversal and splitting of waves in an excitable medium caused by an electric field, Science 257 (1992) 951–954.
[17] H. Ševčíková, I. Schreiber and M. Marek, Dynamics of oxidation Belousov–Zhabotinsky waves in an electric field, J. Phys. Chem. 100 (1996) 19153–19164.
[18] K. Showalter, Chemical waves, in: *Kinetics of Nonhomogeneous Processes*, ed. G.R. Freeman (Wiley, New York, 1987).
[19] D. Snita, J. Lindner, M. Marek and J.H. Merkin, Propagating reaction fronts in an ionic autocatalytic system: the effects of electric field intensity and ionic strength, Math. Comput. Modelling 27 (1998) 1–25.

[20] D. Snita and M. Marek, Transport and reaction in ionic chemical systems, Physica D 75 (1994) 521–540.
[21] D. Snita, H. Ševčíková, J. Lindner, M. Marek and J.H. Merkin, Capillary electrophoresis with chemical reaction: effect of ionic strength, J. Chem. Soc. Faraday Trans. 94 (1998) 213–222.
[22] D. Snita, H. Ševčíková, M. Marek and J.H. Merkin, Ionic autocatalytic reaction fronts in electric fields, J. Phys. Chem. 100 (1996) 18740–18748.
[23] D. Snita, H. Ševčíková, M. Marek and J.H. Merkin, Travelling waves in an ionic autocatalytic chemical system with an imposed electric field, Proc. Roy. Soc. London Ser. A 453 (1997) 2325–2351.